ESEEM and Mims ENDOR Spectroscopies of *cis,trans*-(L-N_2S_2)$Mo^{V}O(SCH_2Ph)$: Detection of the Two Benzylthiolate α Protons

Andrei V. Astashkin,*,† Michele Mader Cosper,‡ Arnold M. Raitsimring,* and John H. Enemark*

Department of Chemistry, University of Arizona, Tucson, Arizona 85721-0041

Received April 10, 2000

Introduction

The crystal structure of sulfite oxidase (SO)[1] shows a distorted square-pyramidal Mo center (Figure 1) with coordination by two oxo groups, the S^{γ} atom from a conserved cysteine residue, and the two sulfur atoms of the pyranopterin dithiolate[2,3] (molybdopterin[4,5]). Although the significance of the coordinated cysteine is not known, it has been suggested that it plays a role in modulating oxygen atom transfer (OAT)[6] and in tuning the redox potential of the site.[7] The sulfite oxidase family[8] of mononuclear Mo enzymes also contains the assimilatory nitrate reductases (NRs) from plants and algae, which are postulated to possess analogous active sites on the basis of the homology of the amino acid sequences[1,9−12] and from XAS data.[13,14]

Continuous-wave (CW) electron paramagnetic resonance (EPR) spectroscopy has been a useful tool for probing the paramagnetic Mo(V) sites of SO and assimilatory NR,[15−19] but hyperfine interactions between the unpaired electron and the β-CH_2 protons of coordinated cysteine residues have not been observed in CW EPR spectra of SO or assimilatory NR. George[20] observed forbidden EPR transitions in the *hpH* form of SO from weakly coupled nonexchangeable protons, which were postulated to be carbon-bound protons of the pyranopterin dithiolate or an amino acid residue.

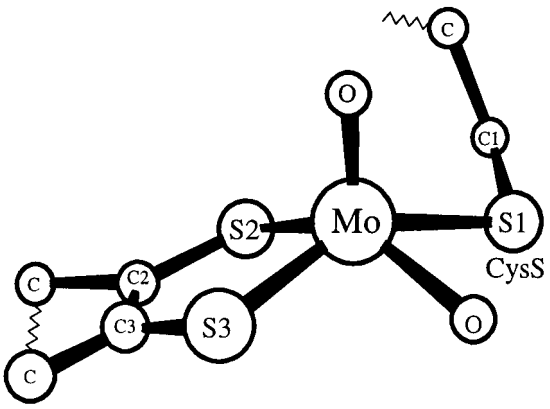

Figure 1. Mo center of chicken liver sulfite oxidase.[1] C1 belongs to the β-CH_2 group of the coordinated cysteine residue.

In principle, any atoms near the Mo(V) center with a nonzero nuclear spin ($I > 0$) can give rise to hyperfine interactions. However, the magnitude of the hyperfine interaction decreases with the distance from the unpaired electron, and the corresponding splittings in the CW EPR spectrum can easily become unresolved. In such a situation, the high-resolution varieties of EPR spectroscopy, including CW and pulsed electron−nuclear double resonance (ENDOR) and electron spin echo envelope modulation (ESEEM), may be utilized. The greater spectral resolution of the pulsed EPR techniques makes them suitable for detection of weak hyperfine interactions. However, our early attempts to detect the β-CH_2 protons of the coordinated cysteine residue in SO using CW ENDOR failed.[21]

In this work, we have addressed the problem of detection of the cysteinyl β-CH_2 protons at the Mo(V) active site in SO (and also in assimilatory NRs from plants and algae and in the periplasmic NRs from *Paracoccus dinitrificans*[22−24] and *Desulfovibrio desulfuricans*[25]) by using the model compound *cis,trans*-(L-N_2S_2)$Mo^{V}O(SCH_2Ph)$[26] (**1**, L-$N_2S_2H_2$ = *N,N′*-dimethyl-*N,N′*-bis(mercaptophenyl)ethylenediamine) (Figure 2). The Mo center in **1** possesses a benzylthiolate ligand, whose α protons mimic the β-CH_2 protons of a coordinated cysteine residue. To detect these weakly coupled protons, the high-resolution pulsed EPR techniques (ESEEM and pulsed ENDOR) were used. Successful detection of the benzylthiolate α protons

* Corresponding authors.
† On leave from the Institute of Chemical Kinetics and Combustion, Russian Academy of Sciences, Novosibirsk 630090, Russia.
‡ Formerly M. L. Mader.

(1) Kisker, C.; Schindelin, H.; Pacheco, A.; Wehbi, W. A.; Garrett, R. M.; Rajagopalan, K. V.; Enemark, J. H.; Rees, D. C. *Cell* **1997**, *91*, 973−983.
(2) Fischer, B.; Enemark, J. H.; Basu, P. *J. Inorg. Biochem.* **1998**, *72*, 13-21.
(3) Hille, R. *JBIC, J. Biol. Inorg. Chem.* **1997**, *2*, 804−809.
(4) Rajagopalan, K. V. *Adv. Enzymol. Relat. Areas Mol. Biol.* **1991**, *64*, 215−290.
(5) Rajagopalan, K. V.; Johnson, J. L. *J. Biol. Chem.* **1992**, *267*, 10199−10202.
(6) Izumi, Y.; Rose, K.; Glaser, T.; McMaster, J.; Basu, B.; Enemark, J. H.; Hedman, B.; Hodgson, K. O.; Solomon, E. I. *J. Am. Chem. Soc.* **1999**, *121*, 10035−10046.
(7) Helton, M. E.; Pacheco, A.; McMaster J.; Enemark, J. H.; Kirk, M. L. *J. Inorg. Biochem.*, submitted for publication.
(8) Hille, R. *Chem. Rev.* **1996**, *96*, 2757−2816.
(9) Crawford, N. M.; Smith, M.; Bellissimo, D.; Davis, R. W. *Proc. Natl. Acad. Sci. U.S.A.* **1988**, *85*, 5006.
(10) Neame, P. J.; Barber, M. J. *J. Biol. Chem.* **1989**, *264*, 20894.
(11) Hyde, G. E.; Campbell, W. H. *Biochim. Biophys. Res. Commun.* **1990**, *168*, 1285.
(12) Wootton, J. C.; Nicholson, R. E.; Cock, J. M.; Walters, D. E.; Burke, J. F.; Doyle, W. A.; Bray, R. C. *Biochim. Biophys. Acta* **1991**, *1057*, 157−185.
(13) Cramer, S. P.; Solomonson, L. P.; Adams, M. W. W.; Mortenson, L. E. *J. Am. Chem. Soc.* **1984**, *106*, 1467−1471.
(14) George, G. N.; Mertens, J. A.; Campbell, W. H. *J. Am. Chem. Soc.* **1999**, *121*, 9730−9731.
(15) Vincent, S. P.; Bray, R. C. *Biochem. J.* **1978**, *171*, 639−647.
(16) Lamy, M. T.; Gutteridge S.; Bray, R. C. *Biochem. J.* **1980**, *185*, 397−403.
(17) Bray, R. C. In *Biological Magnetic Resonance*; Reuben, J., Berliner, L. J., Eds.; Plenum Press: New York, 1980; pp 45−84.
(18) Gutteridge, S.; Lamy, M. T.; Bray, R. C. *Biochem. J.* **1980**, *191*, 285−288.
(19) Bray, R. C.; Lamy, T.; Gutteridge, S.; Wilkinson, T. *Biochem. J.* **1982**, *201*, 241−243.
(20) George, G. N. *J. Magn. Reson.* **1985**, *64*, 384−394.
(21) Raitsimring, A. M.; Basu, P.; Pacheco, A.; LoBrutto, R.; Enemark, J. H. Unpublished results.
(22) Berks, B. C.; Richardson, D. J.; Reilly, A.; Willis, A. C.; Ferguson, S. J. *Biochem. J.* **1995**, *309*, 983−992.
(23) Berks, B. C.; Richardson, D. J.; Robinson, C.; Reilly, A.; Aplin, R. T.; Ferguson, S. J. *Eur. J. Biochem.* **1994**, *220*, 117−124.
(24) Breton, J.; Berks, B. C.; Reilly, A.; Thomson, A. J.; Ferguson, S. J.; Richardson, D. J. *FEBS Lett.* **1994**, *345*, 76−80.
(25) Dias, J. M.; Than, M. E.; Humm, A.; Huber, R.; Bourenkov, G. P.; Bartunik, H. D.; Bursakov, S.; Calvete, J.; Caldeira, J.; Carneiro, C.; Moura, J. J. G.; Moura, I.; Romão, M. J. *Structure* **1999**, *7*, 65−79.
(26) Mader, M. L.; Carducci, M. D.; Enemark, J. H. *Inorg. Chem.* **2000**, *39*, 525−531.

10.1021/ic000405k CCC: $19.00
Published on Web 09/29/2000

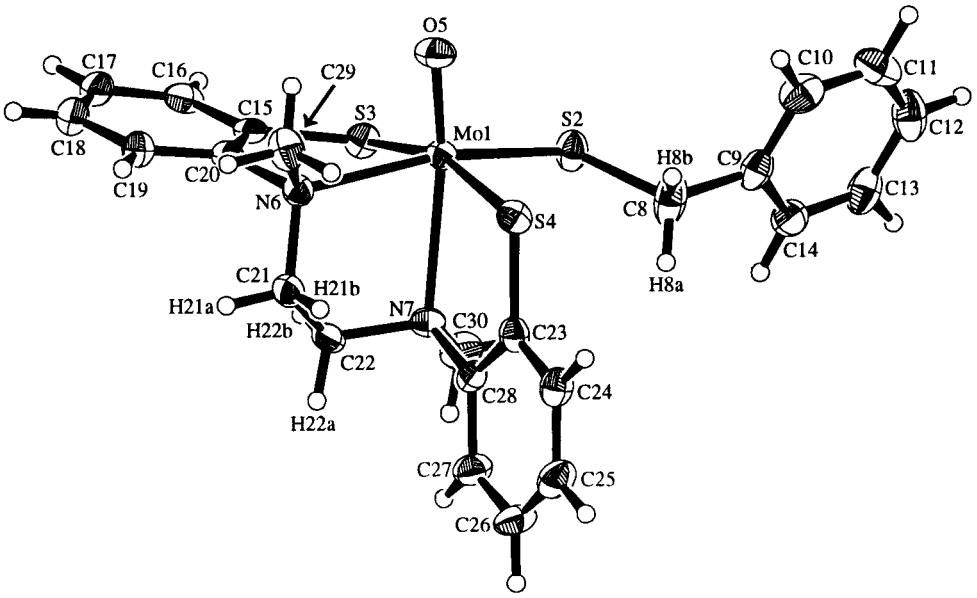

Figure 2. ORTEP diagram of *cis*,*trans*-(L-N_2S_2)$Mo^{V}O(SCH_2Ph)$ (**1**).

was only achieved by selective deuteration of these protons and then taking the difference between the spectra of protonated and deuterated samples. This indicates that a similar approach may be necessary for studying the cysteinyl β-CH_2 protons in SO.

Experimental Section

Materials. The syntheses and characterizations of *cis*,*trans*-(L-N_2S_2)-$Mo^{V}O(SC\mathbf{H}_2Ph)$[26] (**1H**, which is an extended notation for **1** to show that this is the protonated sample), *cis*,*trans*-(L-N_2S_2)$Mo^{V}O(SC\mathbf{D}_2Ph)$[26] (**1D**), and benzyl-α,α-d_2 mercaptan[27] followed previously published procedures.

ESEEM and Pulsed ENDOR Spectroscopies. The pulsed ENDOR and ESEEM experiments were carried out on a home-built X/P-band pulsed EPR spectrometer[28] that was upgraded recently (1999) by a pulsed ENDOR accessory; a temperature of ~20 K was maintained by an Oxford ESR900 cryostat. The primary ESEEM experiments were performed at the microwave (mw) frequency $\upsilon_0 = 8.904$ GHz (X-band). For these experiments, frozen solutions (1.3 mM) of **1H** and **1D** were prepared in a 1:1 mixture of DMF and 1,2-dichloroethane.

The pulsed ENDOR measurements were performed at $\upsilon_0 = 14.91$ GHz (P-band) using the technique developed by Mims.[29] The rectangular TE_{102} resonator used in these measurements was made of 5 μm copper foil supported by a body machined from acrylic plastic. The resonator fit the ESR 900 cryostat after a slight modification of the quartz insert tube. This construction ensured transparency to the radio-frequency (rf) field while keeping the mw power inside the cavity ($Q \sim 300$). Helmholtz rf coils (3.5 turns each) were mounted just outside the resonator, on its top and bottom. The magnetic component of the rf field, $\mathbf{B_2}$, was thus oriented vertically, along the axis of a sample and perpendicular to the external magnetic field $\mathbf{B_0}$. With an rf amplifier (Amplifier Research) output power of about 200 W, the typical duration of the rf pulse providing a 180° flip angle for protons was about 15 μs.

For the ENDOR experiments, frozen solutions (1.3 mM) of **1H** and **1D** were prepared in a 1:1 mixture of dimethylformamide-d_7 (Cambridge Isotope Laboratory) and 1,2-dichloroethane-d_4 (Cambridge Isotope Laboratory). Since the experiments involved subtraction of the spectra taken for **1H** and **1D**, it was important to ensure that the distributions of the mw and rf fields over these samples were similar. With this in mind, the samples for the ENDOR experiments were made of lengths considerably exceeding the height of the mw cavity (13 mm), so that the sample ends were protruding from the cavity in both directions. With this arrangement, the mw and rf fields were strongly inhomogeneous, but their distributions over the samples were the same.

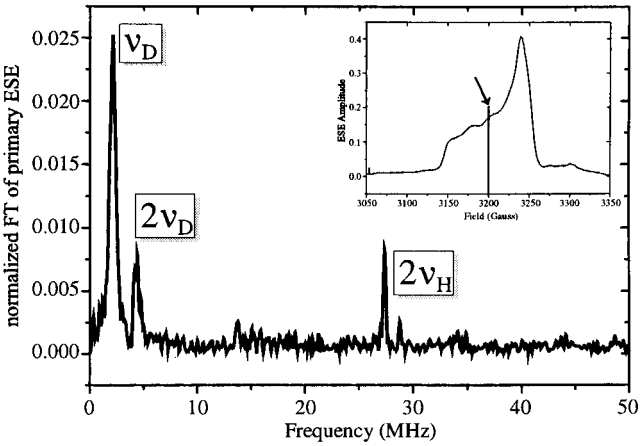

Figure 3. Magnitude FT spectrum of the normalized quotient ESEEM obtained by division of the primary ESEEM of **1D** by that of **1H**. Experimental conditions: $T = 20$ K; $B_0 = 3200$ G; $\upsilon_0 = 8.904$ GHz. Inset: Field-sweep ESE spectrum of **1H** recorded at $\upsilon_0 = 8.904$ GHz. The arrow marks the magnetic field where the ESEEM measurements were performed.

Results

The field-sweep electron spin echo (ESE) spectrum of **1H** detected at $\upsilon_0 = 8.904$ GHz, the frequency of the ESEEM measurements, is shown in the inset of Figure 3. It has turning points at magnetic fields B_0 of 3145 G (g_Z), 3240 G (g_Y), and 3250 G (g_X). At the frequency used for the ENDOR measurements, $\upsilon_0 = 14.91$ GHz (P-band), the spectrum has a similar shape (not shown), with turning points at B_0 values of 5266 G (g_Z), 5426 G (g_Y), and 5442 G (g_X). The principal values of the **g** tensor are $g_X = 1.958$, $g_Y = 1.963$, and $g_Z = 2.023$. The spectrum of **1D** (not shown) was indistinguishable from that of **1H**.

ESEEM Spectroscopy. The primary ESEEMs of **1H** and **1D** (Supporting Information, Figure S1) show a deep modulation

(27) Frank, R. L.; Smith, P. V. *J. Am. Chem. Soc.* **1946**, *68*, 2103.
(28) Borbat, P. P.; Raitsimring, A. M. In *Abstracts of Papers*, 36th Rocky Mountain Conference on Analytical Chemistry, Denver, CO, July 31−Aug 5, 1994; p 94.
(29) Mims, W. B. *Proc. R. Soc. London* **1965**, *A283*, 452−457.

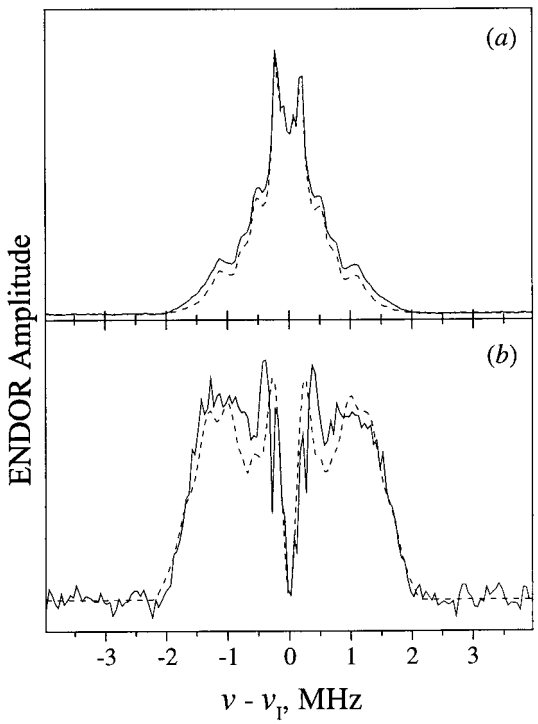

Figure 4. (a) Mims ENDOR spectra of **1H** (solid line) and **1D** (dashed line) at $B_0 = 5272$ G. These spectra were obtained by summing up individual spectra recorded with the time interval τ between the first and second mw pulses ranging from 200 to 1400 ns, in 50 ns increments. Experimental conditions: mw pulse durations, 25 ns (90°); time interval between the second and third mw pulses, 19.75 μs; rf pulse duration, 16.4 μs (180°); $T = 14$ K. (b) Solid line: difference between the spectra shown in panel a. Dashed line: simulation with $\psi = 154°$, $\theta = 310°$, and $\varphi = 23°$ and with θ_{MoS} and θ_{SC} distributed within the limits of 65−100 and 41−82°, respectively.

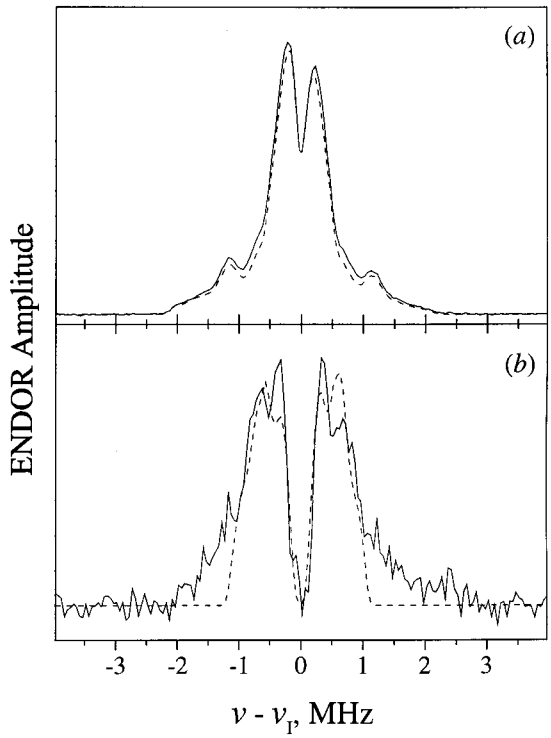

Figure 5. (a) Mims ENDOR spectra of **1H** (solid line) and **1D** (dashed line) at $B_0 = 5448$ G. These spectra were obtained by summing up individual spectra recorded at τ values from 200 to 1400 ns at 50 ns intervals. Other experimental parameters are the same as those for Figure 4. (b) Solid line: difference between the spectra shown in panel a. Dashed line: simulation with parameters listed in the caption to Figure 4.

superimposed on the ESE decay, which arises primarily from the equatorial nitrogen nucleus (N6 in Figure 2). Division of the ESE decay of **1D** by that of **1H** eliminated the ESEEM due to the nitrogen nuclei, matrix protons, and protons of **1H** that were not substituted by deuterons in **1D**. After division, normalization, and subtraction of the nonoscillating background, the primary ESEEM (Supporting Information, Figure S2) contained only the harmonics from the benzylthiolate α protons of **1H** and the α deuterons of **1D**. The Fourier transformation (FT) of the quotient ESEEM yields the spectrum in Figure 3, which shows fundamental (2.10 MHz $\approx \nu_D$, the Zeeman frequency of deuterons in the external magnetic field $B_0 = 3200$ G) and sum combination (4.40 MHz $\approx 2\nu_D$) lines for the deuterons and a sum combination line for the protons (27.32 MHz $\approx 2\nu_H$). The sum combination lines observed for the benzylthiolate protons (deuterons) are slightly shifted from the exact $2\nu_H$ (27.25 MHz) and $2\nu_D$ (4.18 MHz) positions due to the anisotropic hyperfine interaction and, in the case of deuterons, the nuclear quadrupole interaction.

Performing the ESEEM (or ENDOR) measurements at different magnetic fields across the strongly anisotropic EPR spectrum of Mo(V) (Figure 3, inset) allows one to select different orientations of the Mo complex with respect to $\mathbf{B_0}$. However, these measurements did not reveal any noticeable dependence of the intensity of the ESEEM spectral lines on B_0 (not shown). We, therefore, turned to pulsed ENDOR as a method to directly obtain the shapes of the nuclear transition lines (the ENDOR line shapes are often more sensitive to changes in the orientation of $\mathbf{B_0}$ in the molecular coordinate system).

Pulsed ENDOR Spectroscopy. The benzylthiolate α protons of **1** were also detected by Mims ENDOR[29] spectroscopy. The spectra in Figures 4a and 5a were collected at two canonical orientations of the Mo(V) **g** tensor, at $B_0 = 5272$ and 5448 G, respectively. One can see that the difference between the spectra recorded in protonated and deuterated samples is very small and it is not expressed as a single narrow feature. Rather, it is observed as a slight change in intensity of the proton lines distributed over wide areas across the spectra. If the situation for the cysteinyl β-CH_2 protons in SO is similar to that for the α protons of **1**, it is not surprising that we could not detect them with CW ENDOR.[21]

Figures 4b and 5b show the spectra of the benzylthiolate α protons only, obtained as differences between the spectra of protonated and deuterated samples shown in Figures 4a and 5a. The lines seen in the difference spectra clearly show the dependence upon the magnetic field, which translates for this system into the dependence on the orientation of $\mathbf{B_0}$ in the molecular coordinate frame. The shapes of these spectra are complicated, with characteristic widths of about 3 MHz at $B_0 = 5272$ G and about 2 MHz at $B_0 = 5448$ G.

To extract structural information from the experimental spectra, we performed numerical simulations with variations of the geometry of the Mo−S2−C8−H8a,b fragment and orientation of the **g** tensor axes with respect to the M═O and Mo−S2 bonds. Since the H8 protons are three bonds away from the unpaired electron localized on the molybdenum ion, their isotropic hyperfine interaction (hfi) constants were assumed to be zero. The orientations of the **g** tensor axes were defined by three Euler angles, ψ, θ, and φ. The values $\psi = 0°$, $\theta = 0°$, and $\varphi = 0°$ corresponded to the orientation with the g factor axis **X** being parallel to the Mo═O bond and the **Z** axis being

parallel to the Mo−S2 bond. Axis **Y** is perpendicular to **X** and **Z**. The coordinate transformation to nonzero angles was then obtained by first rotating around the Mo−S2 bond by ψ, then rotating around the new *X* axis by θ, and, finally, rotating around the new *Z* axis by φ.

Concerning the Mo−S2−C8−H8a,b fragment, we assumed in our simulations that the dihedral angle θ_{MoS} between the O═Mo−S2 and Mo−S2−C8 planes may have any value or may even be distributed in some limits (ultimately, from 0 to 360°). Similar provisions were made for the dihedral angle θ_{SC} between the Mo−S2−C8 and S2−C8−H8a planes. To calculate the distances from Mo to H8a,b, the Mo−S2 and S2−C8 bond lengths were taken as 2.36 and 1.83 Å, respectively, and the angle between these bonds was 105°.[26] The C8−H8a,b bond lengths were 1.09 Å, and the S2−C8−H8a,b angles were 109°, corresponding to the sp^3 hybridization of the C8 valence orbitals. Without any limitations on the dihedral angles introduced above, the Mo···H8 distance could vary from 3.06 to 4.33 Å, with the corresponding range for the anisotropic hfi constant $T_\perp$ of −2.7 to −0.95 MHz, as calculated by the point dipole approximation. As a result of our calculations, we obtained a reasonable fit to the experimental spectra for $\psi = 154°$, $\theta = 310°$, and $\varphi = 23°$, with θ_{MoS} and θ_{SC} distributed within the limits of 65−100 and 41−82°, respectively. It is interesting to note that, in the crystal structure of **1** (Figure 2), $\theta_{MoS} = 105°$ and $\theta_{SC} = 76°$, i.e., values close to the limits found in our simulation. In frozen solution, however, as our simulation shows, the whole side chain has a certain degree of freedom.

Within the range of conformations of the Mo−S2−C8−H8a,b fragment estimated from our ENDOR simulations, $T_\perp$ varies from −2.3 to −1.6 MHz. This range of $T_\perp$ values obtained from the ENDOR simulations agrees with the ESEEM data. Indeed, the intensity of the proton sum combination line due to H8a,b in the ESEEM spectrum shown in Figure 3 is about 0.0075. This intensity allows one to independently estimate the effective value of $T_\perp$, which we will do, for simplicity, in the approximation of the orientationally disordered system. As follows from ESEEM theory,[30] the amplitude $I_{2\nu_H}$ of the sum combination line in the normalized ESEEM spectrum is equal to $[9T_\perp \sin\theta \cos\theta/(4\nu_H)]^2$, where θ is the angle between $\mathbf{B_0}$ and the anisotropic hfi axis. After averaging over θ, this results in $I_{2\nu_H} = 0.3[T_\perp/\nu_H]^2$ for a single proton. Taking into account that, in our case, two protons contribute to the sum combination line, we can find $I_{2\nu_H} \cong 0.0075/2 \cong 0.0037$. With $\nu_H \cong 13.6$ MHz, this immediately results in $T_\perp \cong 1.5$ MHz, well within the limits obtained from the ENDOR spectra. The shift of the sum combination line from the exact $2\nu_H$ position is equal to $\Delta\nu \cong T_\perp^2/2\nu_H$,[30] which, for $T_\perp \cong 1.5$ MHz, gives $\Delta\nu \cong 0.08$ MHz, in good agreement with the value observed in our experiment (∼0.07 MHz). These data are also in agreement with the ESEEM amplitude and damping for the benzylthiolate α deuterons (Figure S2 in the Supporting Information).

(30) Dikanov, S.; Tsvetkov, Y. *Electron Spin Echo Envelope Modulation (ESEEM) Spectroscopy*; CRC Press: Boca Raton, FL, 1992.

Discussion

The benzylthiolate α protons of **1** were detected by ESEEM and Mims ENDOR spectroscopy in difference experiments on compounds containing the SC**H**$_2$Ph and SC**D**$_2$Ph ligands. The results presented here indicate that direct detection of the β-CH_2 protons in the side chain of a coordinated cysteine residue will require difference experiments using native SO and protein in which the cysteinyl β-CH_2 protons have been substituted by deuterons. Expression of the enzyme in the presence of L-cysteine-*3,3-d*$_2$ will label all four cysteine residues with deuterons at the β-C positions, but only the β-CH_2 protons (or deuterons) of the coordinated cysteine residue are sufficiently close to the unpaired electron on the Mo center to be detectable by ESEEM or pulsed ENDOR spectroscopy.

The conserved cysteine residue at the Mo active site of SO is essential for catalytic activity, and the human C207S mutant has been shown to have severely diminished activity.[31] The exact role of the coordinated cysteine residue is not known. XAS studies of (tp*)$Mo^{VI}O_2X$ (X = Cl, SCH_2Ph, OPh) and DFT calculations on related model compounds by Izumi et al.[6] indicate that the Mo−SR torsional angle modulates the relative electrophilicities of the two oxo groups of the $[Mo^{VI}O_2]^{2+}$ center. It was suggested that, for SO, the O_{ax}−Mo−S_{cys}−CH_2 dihedral angle could act as a switch during catalytic turnover to electronically facilitate selective transfer of one of the oxo ligands. The orientation of the cysteinyl β-CH_2 protons is changed as the O_{ax}−Mo−S_{cys}−CH_2 torsional angle is varied. Hence, probing the orientational dependence of the hyperfine interaction of cysteinyl β-CH_2 protons by pulsed EPR spectroscopy under different conditions could lead to better understanding of the role of the conserved cysteine residue in the proposed reaction mechanisms of SO[32−34] and NRs.[8,14,35]

Acknowledgment. We thank Mr. John Jephson of Circuit Foil Trading for the free sample 5 μm Cu foil used in the construction of the ENDOR cavity and Dr. V. Kozlyuk for invaluable assistance with the pulsed EPR experiments. The spectrometer described in ref 28 and the pulsed ENDOR accessory were constructed under NSF Grants BIR-922443 and DIR-9016385. Financial support from the National Institutes of Health (Grant #GM37773) is also gratefully acknowledged.

Supporting Information Available: Primary ESEEM spectra for **1H** and **1D**. This material is available free of charge via the Internet at http://pubs.acs.org.

IC000405K

(31) Garrett, R. M.; Rajagopalan, K. V. *J. Biol. Chem.* **1996**, *271*, 7387−7391.
(32) Pacheco, A.; Hazzard, J. T.; Tollin, G.; Enemark, J. H. *JBIC, J. Biol. Inorg. Chem.* **1999**, *4*, 390−401.
(33) Brody, M. S.; Hille, R. *Biochemistry* **1999**, *38*, 6668−6677.
(34) Astashkin, A. V.; Mader, M. L.; Pacheco, A.; Enemark, J. H.; Raitsimring, A. M. *J. Am. Chem. Soc.* **2000**, *122*, 5294−5302.
(35) Butler, C. S.; Charnock, J. M.; Bennett, B.; Sears, H. J.; Reilly, A. J.; Ferguson, S. J.; Garner, C. D.; Lowe, D. J.; Thomson, A. J.; Berks, B. C.; Richardson, D. J. *Biochemistry* **1999**, *38*, 9000−9012.